Construction of a micro-nano reactor assembled by TiO$_2$/N-C ultrathin sheets for photocatalytic H$_2$ evolution

Yu Wang,[†a] Wenwen Zhan,[†a] Lei Yang,[b] Jianwei Zhao,[b] Liming Sun,[*a] Xiaojun Wang[a] and Xiguang Han[*a]

[a] Jiangsu Key Laboratory of Green Synthetic Chemistry for Functional Materials, Department of Chemistry, School of Chemistry and Chemical Engineering, Jiangsu Normal University, Xuzhou, 221116, China

[b] Shenzhen HUASUAN Technology Co., Ltd, Shenzhen, 518055, China

1. Experimental Detail

1.1 Preparation of NH$_2$-MIL-125 hexahedron

The NH$_2$-MIL-125 hexahedron is synthesized using tetraisopropyl titanate (TIPT) as the Ti salt and 2-aminoterephthalic acid as the organic linker by a simple hydrothermal method at 150 °C for 24 h. After the autoclave cooled to room temperature naturally, samples were collected by centrifugation, thoroughly washed with ethanol 3-4 times, and dried at 60 °C.

1.2 Preparation of TiO$_2$/N-C HHUS

We use as-prepared NH$_2$-MIL-125 hexahedron as the precursor. Typically, 10 mg NH$_2$-MIL-125 was add to 10 mL C$_2$H$_5$OH. The suspension was transferred to a Teflon-lined autoclave and heated at 200 °C for 10 h to obtain the MOFs@TiO$_2$ HHUS. After the autoclave cooled to room temperature naturally, the MOFs@TiO$_2$ HHUS were collected by centrifugation, thoroughly washed with distilled water 3-4 times, and dried

at 60 °C. Finally, TiO$_2$/N-C HHUS was synthesized via calcination of the MOFs@TiO$_2$ HHUS at 550 °C for 2 h in Ar gas atmosphere with heating rate of 5 °C·min^{-1}.

1.3 Preparation of TiO$_2$/N-C HHS

First, 10 mg of as-prepared NH$_2$-MIL-125 was added to 10 mL C$_2$H$_5$OH and 95 μL of deionized water. The suspension was then transferred to a teflon-lined autoclave and heated at 200 °C for 6 hours to obtain the MOFs@TiO$_2$ HHS. After the autoclave cooled to room temperature naturally, samples were collected by centrifugation, thoroughly washed with distilled water 3-4 times, and dried at 60 °C. Finally, TiO$_2$/N-C HHS was synthesized via calcination of the MOFs@TiO$_2$ HHS at 550 °C for 2 h in Ar gas atmosphere with heating rate of 5 °C•min^{-1}.

1.4 Preparation of TiO$_2$/N-C FH

First, 10mg of as-prepared NH$_2$-MIL-125 was added to 10 mL C$_2$H$_5$OH and 105 μL of deionized water. The suspension was then transferred to a teflon-lined autoclave and heated at 200 °C for 6 hours to obtain the MOFs@TiO$_2$ FH. After the autoclave cooled to room temperature naturally, the MOFs@TiO$_2$ FH were collected by centrifugation, thoroughly washed with distilled water 3-4 times, and dried at 60 °C. Finally, TiO$_2$/N-C FH was synthesized via calcination of the MOFs@TiO$_2$ FH at 550 °C for 2 h in Ar gas atmosphere with heating rate of 5 °C·min^{-1}.

1.5 Preparation of TiO$_2$ HHUS

The as-prepared MOFs@TiO$_2$ HHUS were calcined for 2 h under O$_2$ gas atmosphere of 5 °C·min^{-1} to synthesize TiO$_2$ HHUS.

1.6 Preparation of TiO$_2$/N-C cube

TiO$_2$/N-C was synthesized by calcination of NH$_2$-MIL-125 under Ar gas atmosphere of 5 ^{o}C·min^{-1} for 2h.

1.7 Characterization

The composition and phase of the as-prepared products were acquired by the powder X-ray diffraction (XRD) pattern using a Panalytical X-pert diffractometer with CuKα radiation. The morphology and crystal structure of as-prepared products were observed by scanning electron microscopy (SEM, SU8100), and high-resolution transmission electron microscopy (HRTEM, FEI Tecnai-F20) with an acceleration voltage of 200 kV. All TEM samples were prepared from depositing a drop of diluted suspensions in ethanol on a carbon film coated copper grid. PHI QUANTUM2000 photoelectron spectrometer (XPS) was using to characterize the surface compositions of product. The surface areas of these samples were measured by the Brunauer-Emmett-Teller (BET) method using nitrogen adsorption and desorption isotherms on a Micrometrics ASAP 2020 system.

1.8 Photoelectric measurement

Photoelectrochemical measurements were performed in a homemade three electrode quartz cell with a PAR VMP3 Multi Potentiostat apparatus. A Pt plate was used as the counter electrode, and Hg/HgCl$_2$ electrode was used as the reference electrode. The working electrode was prepared on fluorine-doped tin oxide (FTO) glass that was cleaned by ultrasonication in a mixture of ethanol and acetone for 10 min and dried at 60 °C. Typically, 10 mg of the sample powder was ultrasonicated in 0.2 mL of ethanol to disperse it evenly to get a slurry. The slurry was spread onto FTO glass,

whose side part was previously protected using Scotch tape. After air drying, the Scotch tape was unstuck. Then, the working electrode was further dried at 150 °C for 2 h to improve adhesion. The exposed area of the working electrode was $2.5cm^2$. The electrochemical impedance spectroscopy (EIS) measurement was carried out using a CHI-760E workstation, in the three electrode cell the electrolyte were 0.025M KH_2PO_4 and 0.025M Na_2HPO_4 standard buffer solution (25℃, pHs = 6.864) without an additive under open circuit potential conditions. The visible light irradiation source was a 300 W Xe arc lamp system. The cathodic polarization curves were obtained using the linear sweep voltammetry (LSV) technique with a scan rate of 100 mV s^{-1}. Photocurrent densities of the samples were measured at 0.2 V versus Hg/Hg_2Cl_2 under non-illuminated (i.e. dark) and illuminated (i.e. light) conditions.

1.9 Photocatalytic activity test

The photocatalytic reaction was carried out in a gas-closed system with a reactor made of quartz. A 300 W xenon lamp was used as a light source. The distance between the lamp and the reactor is 3 cm. In a typical experiment, the photocatalyst (5 mg) was added into the aqueous solution (8 mL) containing triethanolamine (TEOA) (8 vol%). The mixture was sonicated for 5 min to form a homogeneous suspension. Then, N_2 was bubbled in the suspension for 30 min. After the gas-closed system was vacuumed, the suspension was irradiated. The amounts of hydrogen produced were measured with a gas chromatograph (GC-7900, China, molecular sieve 5A, TCD) using N_2 as a carrier gas.

1.10   Calculation details

All theoretical calculations were carried out in the Cambridge Sequential Total Energy Package (CASTEP) code,[1] based on plane-wave pseudopotential method.[2] The exchange-correlation effects were described by the local density approximation (LDA).[3] The electron-ion interactions were treated by ultrasoft pseudopotential.[4] Γ and $2\times2\times1$ points were used as a Morkhost-Pack mesh[5] of k-points for geometry optimization and calculating electronic properties. The self-consistent convergence accuracy, the convergence criterion for the force between atoms, and the maximum displacement were set at 2×10^{-5} eV/atom, 5.0×10^{-2} eV/Å, and 2×10^{-3} Å, respectively. The cutoff energy was set to 300 eV.

$5\times3\sqrt{3}$ single graphite (001) layer containing 60 carbon atoms were used to match a (3×3) two TiO_2 molecule layers stoichiometric TiO_2 (001) surface slab containing 18 Ti and 36 O atoms with one bottom molecule layer fixed at the bulk position ($11.77\times12.02\times18.90$ Å^3), forming the graphite (001)/TiO_2 (001)-2TO interface. The graphite (001)/TiO_2 (001)-3TO interface was formed by $5\times3\sqrt{3}$ single graphite (001) layer containing 60 carbon atoms and a (3×3) three TiO_2 molecule layers stoichiometric TiO_2 (001) surface slab containing 27 Ti and 54 O atoms with two bottom molecule layers fixed at the bulk position ($11.77\times12.02\times21.24$ Å^3). The graphite (001)/TiO_2 (001)-4TO interface was formed by $5\times3\sqrt{3}$ single graphite (001) layer containing 60 carbon atoms and a (3×3) four TiO_2 molecule layers stoichiometric TiO_2 (001) surface slab containing 36 Ti and 72 O atoms with three bottom molecule layers fixed at the bulk position ($11.77\times12.02\times23.54$ Å^3).

The formation energies of graphite (001)/TiO_2 (001) interface with different

number of TiO_2 molecular layers were calculated as

$$E_f = E_{interface} - E_{graphite} - E_{TiO_2}$$

where $E_{interface}$, $E_{graphite}$ and E_{TiO_2} represented the total energy of the graphite (001)/TiO_2 (001) interface, graphite (001) surface and TiO_2 (001) surface with different number of TiO_2 molecule layers, respectively.
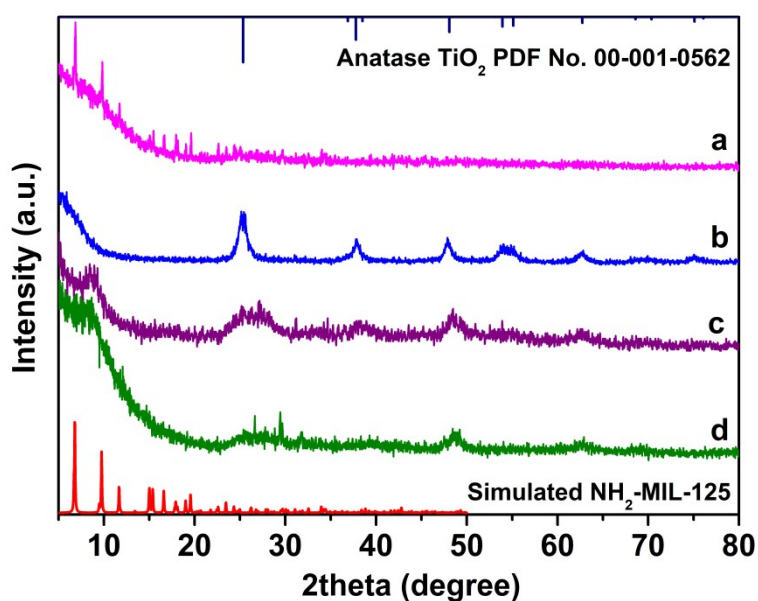
2. Experimental Results

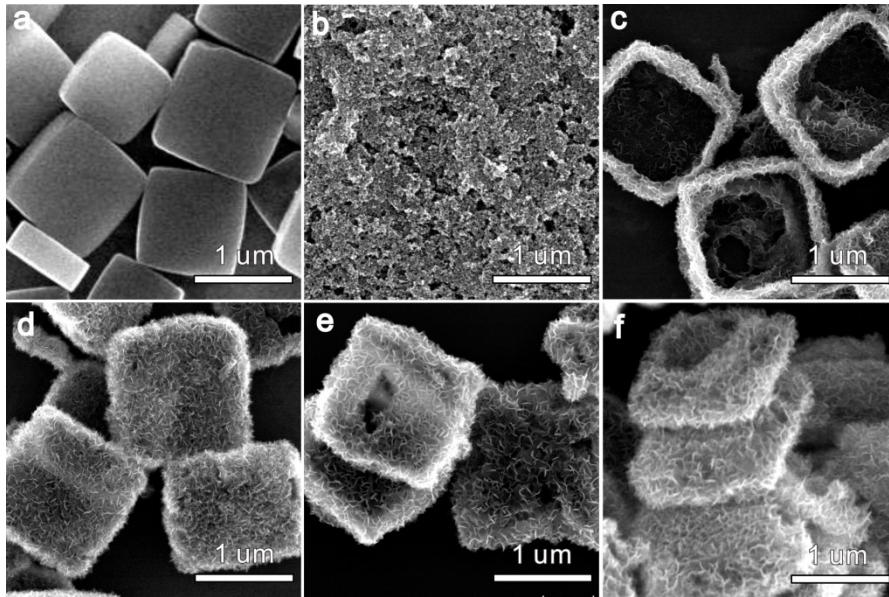Figure S1 XRD patterns of NH_2-MIL-125 hexahedron (a), TiO_2 fragments (b), MOFs@TiO_2 HHS (c), and MOFs@TiO_2 HHUS (d).

Figure S2 SEM images of NH$_2$-MIL-125 (a), the products of NH$_2$-MIL-125 in H$_2$O (b), MOFs@TiO$_2$ FH (c), MOFs@TiO$_2$ HHS-1 (d), MOFs@TiO$_2$ HHS-2 (e), and MOFs@TiO$_2$ HHUS (f).

The experimental results showed that the NH$_2$-MIL-125 hexahedron (Figure S1a) with smooth surface (Figure S2a) would be etched into anatase TiO$_2$ fragments (Figure S2b and Figure S1b) by H$_2$O after hydrothermal reaction at 200 °C for 10 hours. When H$_2$O in the hydrothermal reaction was replaced with the mixture of ethanol and H$_2$O, it was found that the etching degree of NH$_2$-MIL-125 was obviously weakened under the same reaction conditions (200 °C, 10h). With the increase of ethanol proportion in the mixture, part of NH$_2$-MIL-125 was converted into anatase TiO$_2$ (Figure S1c), and then obtained MOFs@TiO$_2$ frame (hollow hexahedron without bottom surfaces, MOFs@TiO$_2$ FH, Figure S2c) and MOFs@TiO$_2$ hollow hexahedron (MOFs@TiO$_2$ HHS-1, Figure S2d) and MOFs@TiO$_2$ HHS-2 (Figure S2e). Through further observation and comparison of Figure S2d and S2e, it was found that increasing the ethanol proportion would make the nanosheets formed by etching on the surface of

MOFs@TiO$_2$ HHS-2 tend to be larger and thinner than that on the surface of MOFs@TiO$_2$ HHS-1. After substituting the mixture of ethanol and H$_2$O by pure ethanol, the obtained alcoholysis product was still MOFs@TiO$_2$ hollow hexahedron (MOFs@TiO$_2$ HHUS, Figure S1d). Different from MOFs@TiO$_2$ HHS, the nanosheets on the surface of MOFs@TiO$_2$ HHUS continued to become large and thin (Figure S2f). The thickness and size of nanosheets subunits of the MOFs@TiO$_2$ hollow hexahedron could be achieved by adjusting the ethanol/H$_2$O rate in the solvent, which could be attributed to the slower alcoholysis rate of NH$_2$-MIL-125 in ethanol than that in H$_2$O.
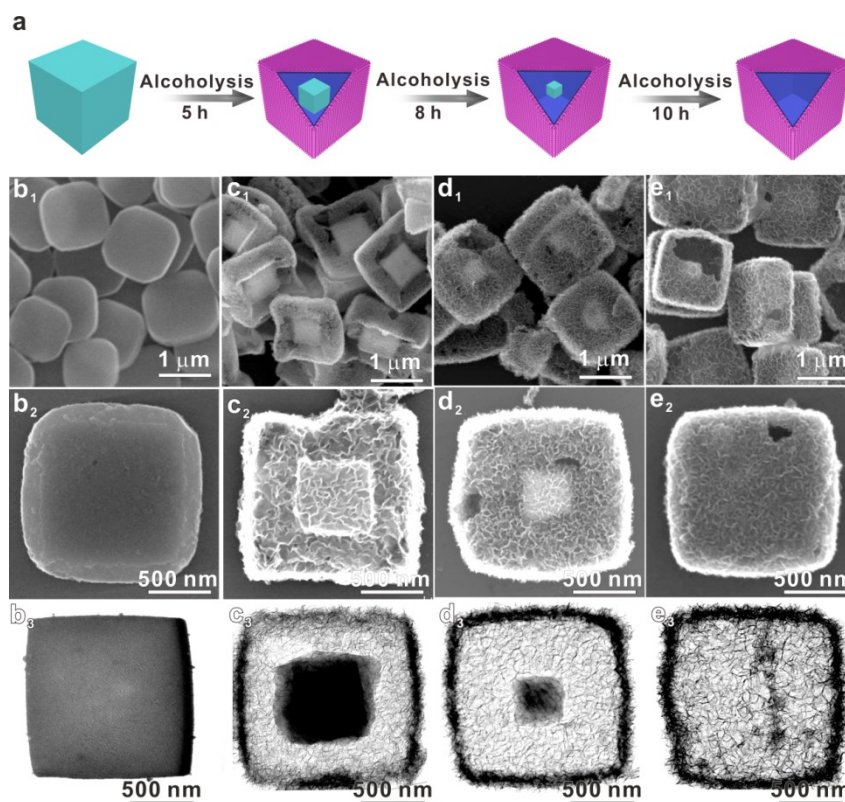
Figure S3 (a) Illustration of the formation process of monodisperse MOFs@TiO$_2$ HHUS; (b$_1$-e$_1$, b$_2$-e$_2$) SEM images of the products of NH$_2$-MIL-125 in ethanol at 200 °C for different reacted time; (b$_3$-e$_3$) TEM images of the products of NH$_2$-MIL-125 in ethanol at 200 °C for different reacted time.
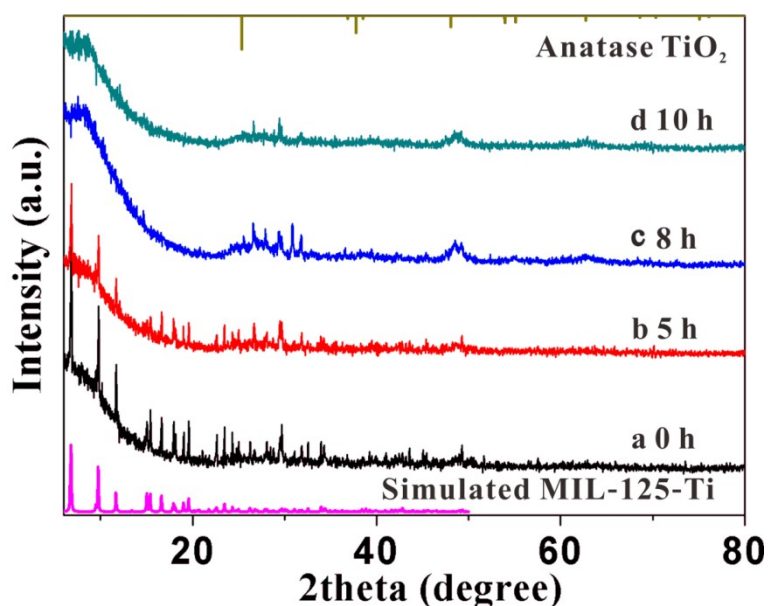
Figure S4 XRD patterns of the products of NH_2-MIL-125 in ethanol at 200 °C for different reacted time.

The time-dependent evolution of NH_2-MIL-125 alcoholysis process were elucidated by power X-ray diffraction (XRD), scanning electron microscope (SEM) and transmission electron microscopy (TEM). The formation process of $MOFs@TiO_2$ HHUS was reasonable illustrated in Figure S3a. The NH_2-MIL-125 precursor with solid hexahedron morphologies had been synthesized by simple solvothermal method (Figure $S3b_1$-b_3, Figure S4a). After alcoholysis in ethanol at 200 °C for 5h, the product retained well the size and hexahedron morphology (Figure $S3c_1$-c_3). But the surface of this product became rough and was decorated with ultra-thin nanosheets, which mainly attributed to the incomplete alcoholysis of NH_2-MIL-125 and partially transformation into anatase TiO_2 phase (Figure S4b). In addition, the hexahedron with core-shell structure was formed during this period of time. With the increase of reacted time to 8 h, the core in the middle of hexahedron decreased gradually (Figure $S3d_1$-d_3), and the anatase TiO_2 phase was more obvious (Figure S4c). The inner core disappeared,

forming the MOFs@TiO$_2$ hollow hexahedron structure assembled by ultra-thin nanosheets (Figure S3e$_1$-e$_3$, Figure S4d). Based on the above data, it was shown that the alcoholysis of NH$_2$-MIL-125 produced anatase TiO$_2$, and the process of alcoholysis began with the surface of NH$_2$-MIL-125 hexahedron and then extended to its interior. Finally, MOFs@TiO$_2$ hollow hexahedron assembled by ultra-thin nanosheets was achieved.
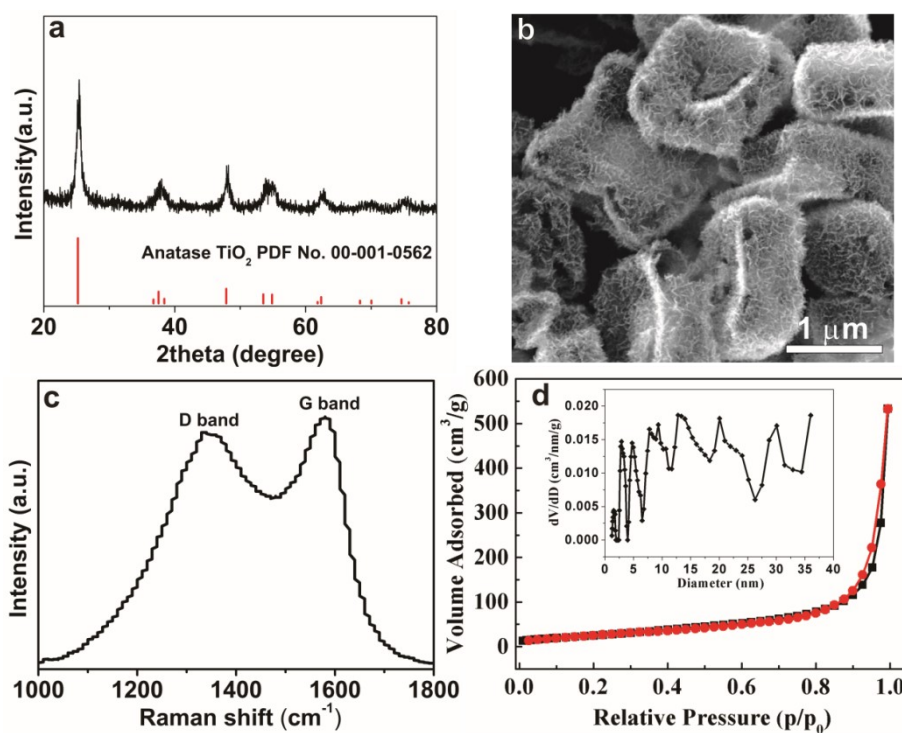

Figure S5 (a) XRD patterns of TiO$_2$/N-C HHUS, (b) SEM image of TiO$_2$/N-C HHUS, (c) Raman spectrum of TiO$_2$/N-C HHUS, (d) N$_2$ adsorption/desorption isotherms and pore size distribution of TiO$_2$/N-C HHUS.
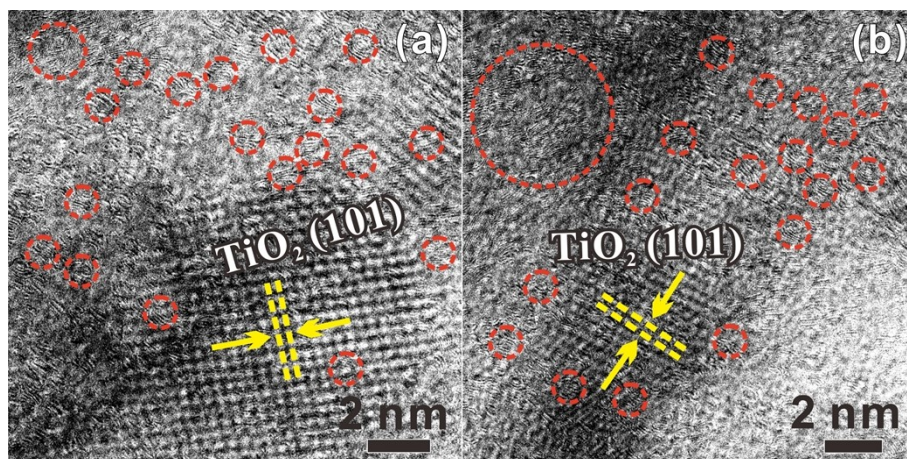
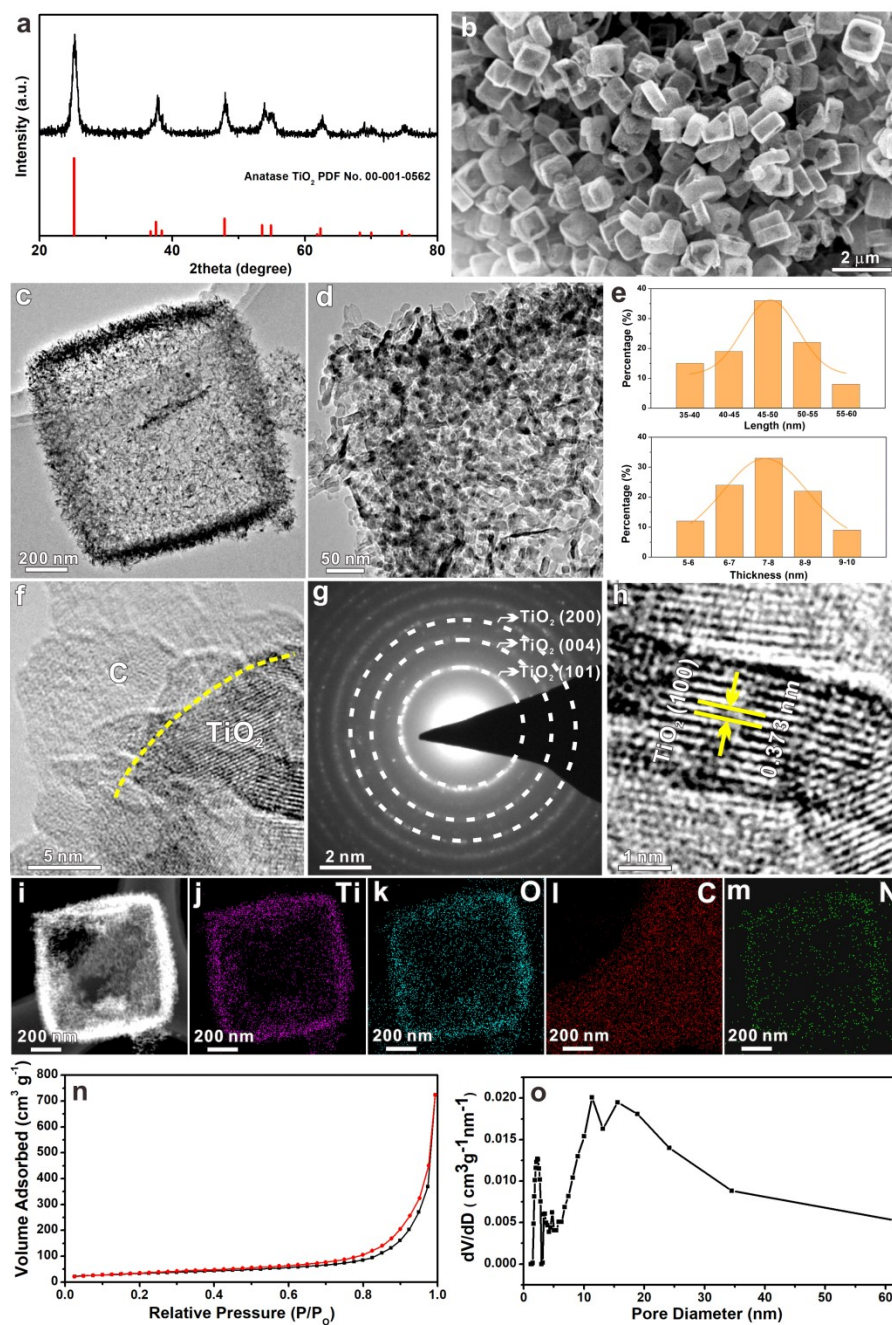Figure S6. HRTEM images of TiO$_2$/N-C HHUS.

Figure S7 (a) XRD patterns of TiO$_2$/N-C HHS, (b) SEM image of TiO$_2$/N-C HHS, (c) TEM image of a single TiO$_2$/N-C HHS, (d) magnified TEM image of a single TiO$_2$/N-C HHS, (e) particle size distribution diagram of nanosheets subunits of TiO$_2$/N-C HHS, (f) magnified TEM of TiO$_2$/N-C HHS, (g) the corresponding SAED pattern, (h) HRTEM image of TiO$_2$/N-C HHS, (i-m) the STEM image and EDX elemental mapping of Ti, O, C and N, N$_2$ adsorption/desorption isotherms (n) and pore size distribution (o) of TiO$_2$/N-C HHS.

XRD pattern of the calcined product of MOFs@TiO$_2$ HHS was shown in Figure S7a. It can be found that all diffraction peaks could be indexed to be anatase TiO$_2$ (PDF No. 00-001-0562), indicating that all residua NH$_2$-MIL-125 in MOFs@TiO$_2$ HHS have been converted into anatase TiO$_2$. SEM image (Figure S7b) showed that this calcined product retained the hollow hexahedron structure of the MOFs@TiO$_2$ HHS precursor. The detailed morphological and structural features of the calcined product of MOFs@TiO$_2$ HHS were further characterized by TEM. Figure S7c verified the hollow hexahedron structure of the calcined product of MOFs@TiO$_2$ HHS. From the magnified TEM (Figure S7d), it could be seen that the hollow hexahedron was composed of many nanosheets. The particle size distribution diagram (Figure S7e) showed that the length and thinckness of these nanosheet subunits were concentrated at 45-50 nm and 7-8 nm, respectively. The interface between TiO$_2$ and carbon layer can be clearly seen in the local magnified TEM of nanosheet subunit (Figure S7f). The selected-area electron diffraction (SAED) patterns (Figure S7g) confirmed the existence of anatase TiO$_2$ in the nanosheets subunits. In the high-resolution TEM (HRTEM) image (Figure S7h), the crystal plane with the *d*-spacing of 0.373 nm could be ascribed to anatase TiO$_2$ (100) plane. The structure and composition of the calcined product of MOFs@TiO$_2$ HHS were further study by scanning transmission electron microscopy (STEM) and elemental mapping. As Figure S7i-m shown, in addition to Ti, O and C elements, N elements were also uniformly distributed in the calcined hollow hexahedron structure. It is preliminarily inferred that these N elements were doped in the carbon layer. Based on the above characterization results, it could be concluded that

the calcined product of MOFs@TiO_2 HHS was hollow hexahedron assembled by TiO_2 nanosheets uniformly coated with N-doped carbon layer (TiO_2/N-C HHS). The N_2 adsorption/desorption isotherms (Figure S7n) and pore size distribution (Figure S7o) showed that the surface area of TiO_2/N-C HHS was 162.9 m^2/g and the pore size distribution belongs to mesoporous range.
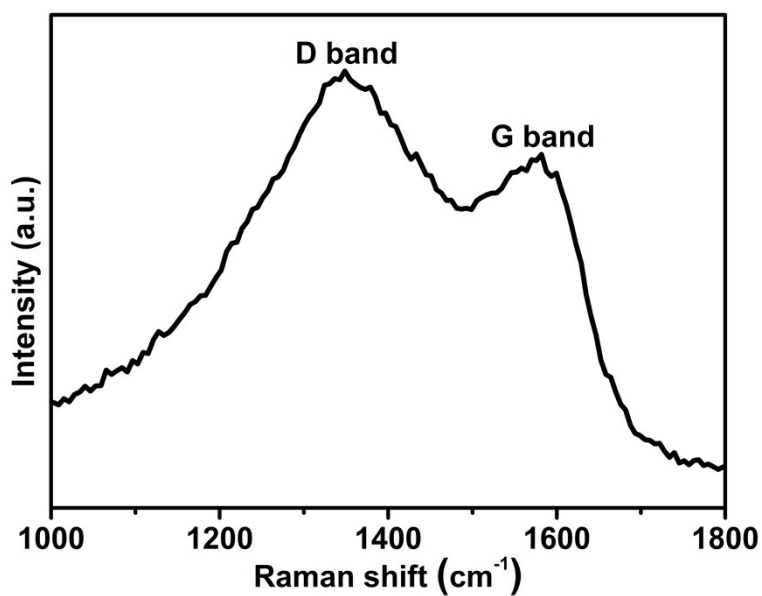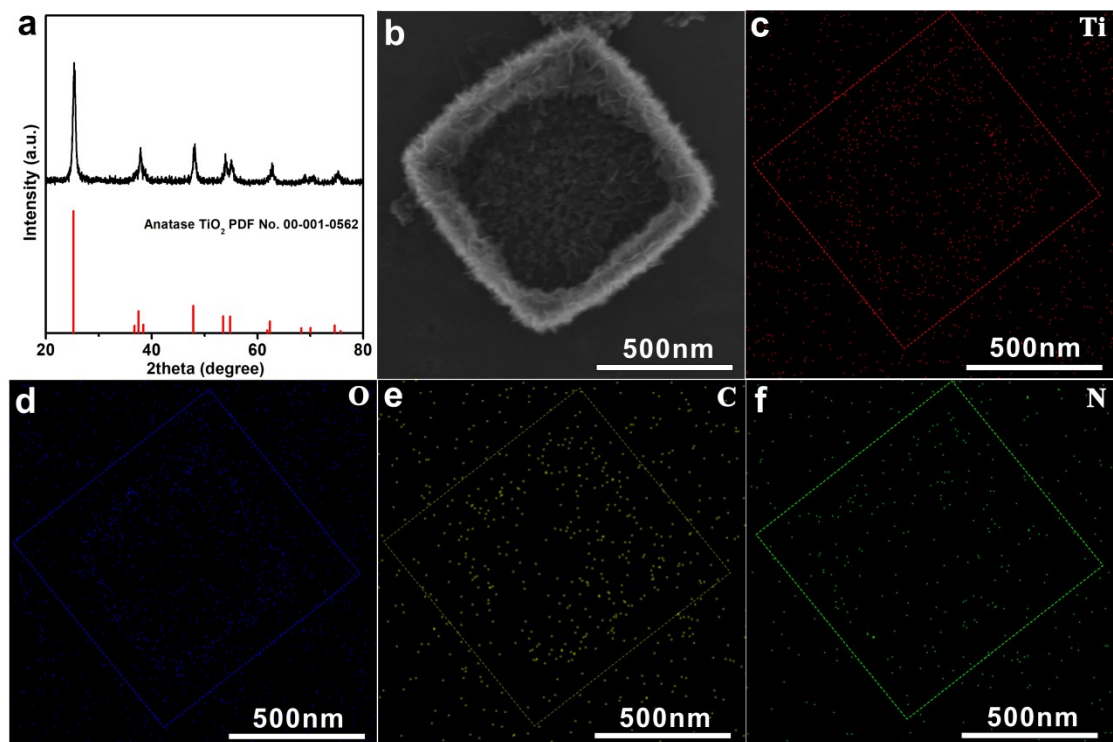

Figure S8 Raman spectrum of TiO_2/N-C HHS.

Figure S9 (a) XRD patterns of TiO$_2$/N-C FH, (b) the STEM image of TiO$_2$/N-C FH, (c-f) EDX
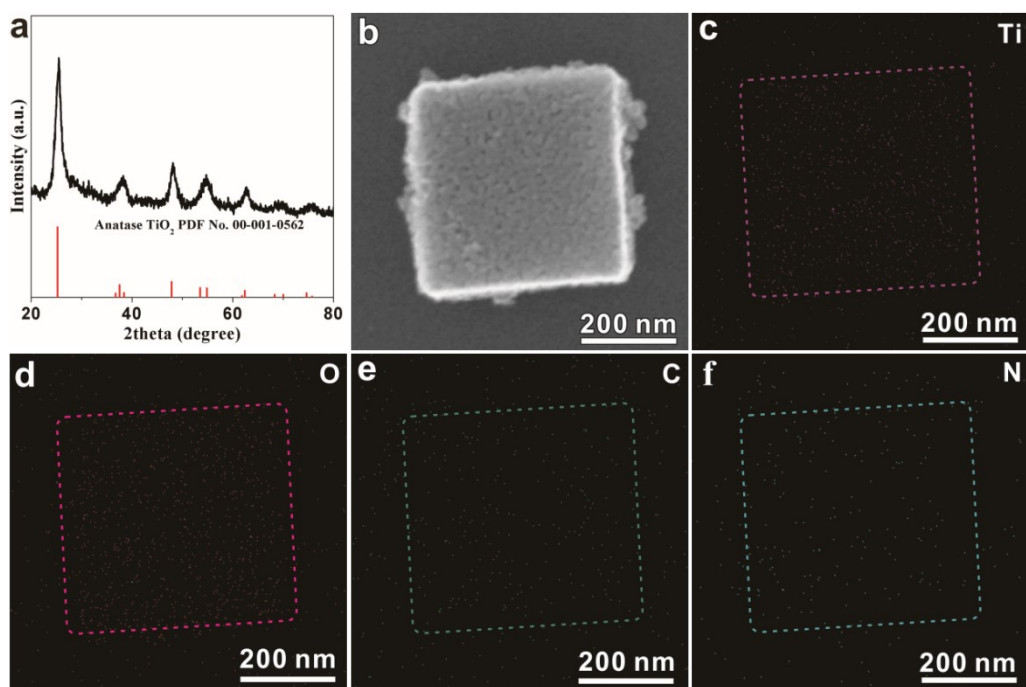
elemental mapping of Ti, O, C and N.

Figure S10 (a) XRD patterns of TiO$_2$/N-C cube, (b) the STEM image of TiO$_2$/N-C cube, (c-f) EDX

elemental mapping of Ti, O, C and N.

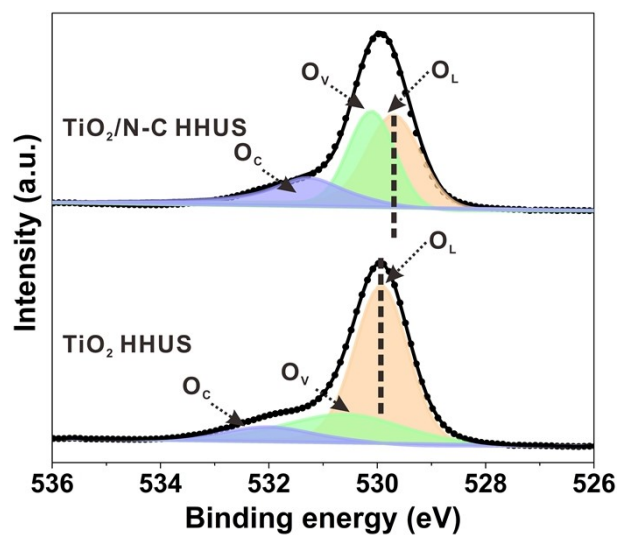Figure S11. Comparison in O 1s XPS spectra between TiO$_2$/N-C HHUS and TiO$_2$ HHUS.

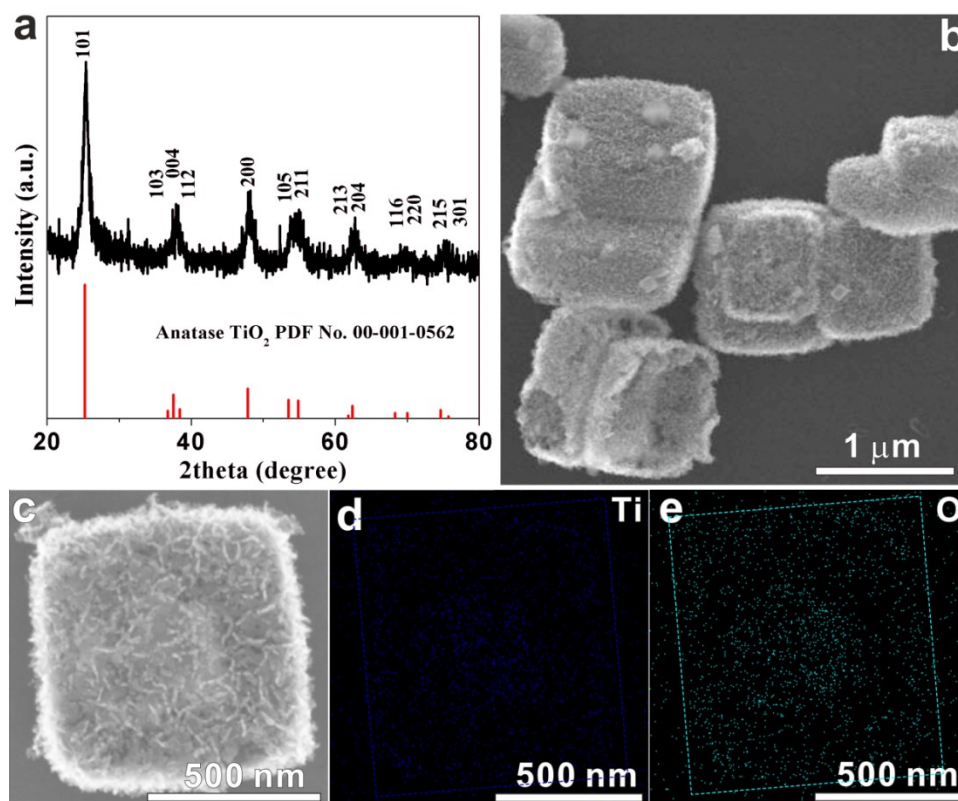Figure S12 (a) XRD patterns of TiO$_2$ HHUS, (b) the STEM image of TiO$_2$ HHUS, (c-f) EDX elemental mapping of Ti and O.
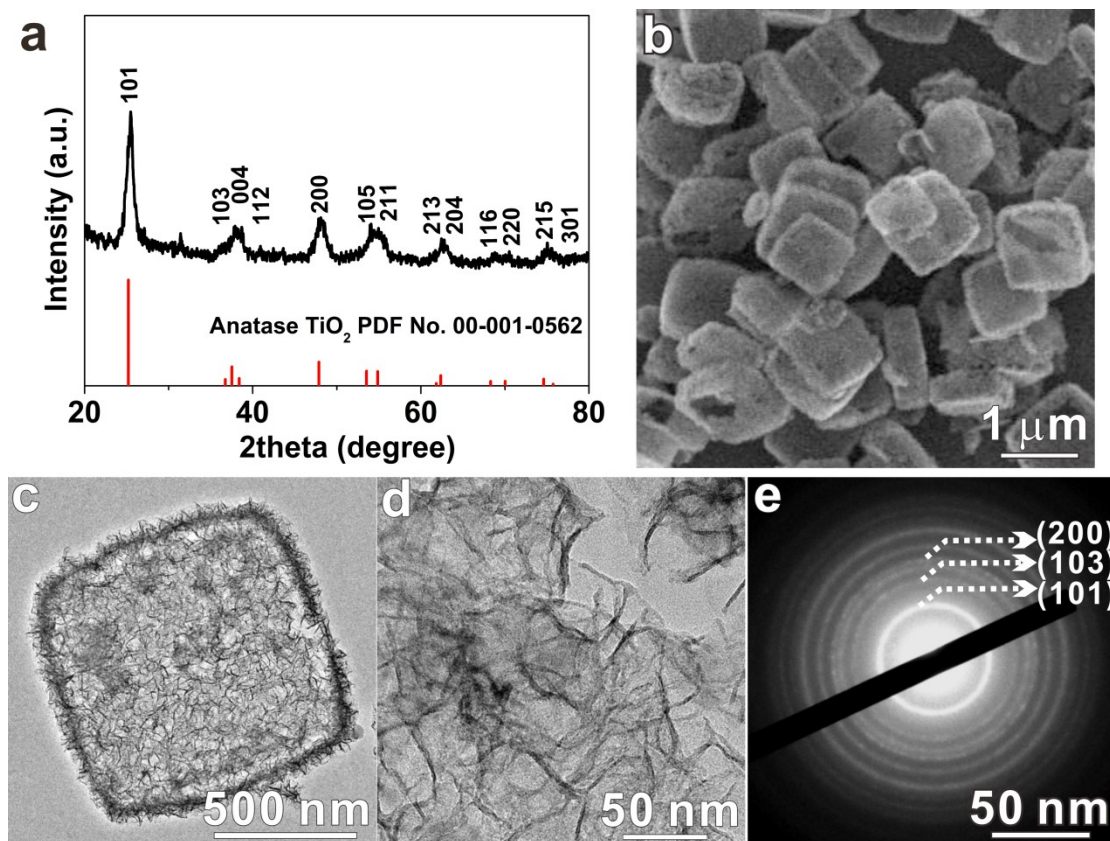
Figure S13 (a) XRD patterns of TiO_2/N-C HCUS after five-cycle catalytic reaction, (b) SEM image of TiO_2/N-C HCUS after five-cycle catalytic reaction, (c,d) TEM image of TiO_2/N-C HCUS after five-cycle catalytic reaction, (e) the corresponding SAED pattern.

References

1. G. H. Du, Q. Chen, P. D. Han, Y. Yu and L. M. Peng, Potassium titanate nanowires: Structure, growth, and optical properties. *Phys. Rev. B* 2003, **67**, 035323.

2. S. J. Clark, M. D. Segall, C. J. Pickard, P. J. Hasnip, M. J. Probert, K. Refon and M. C. Payne, First principles methods using CASTEP. *Z. Kristallogr.* 2005, **220**, 567.

3. D. M. Ceperley and B. J. Alder, Ground state of the electron gas by a stochastic method. *Phys. Rev. Lett.* 1980, **45**, 566.

4. A. M. Rappe, K. M. Rabe, E. Kaxiras and J. D. Joannopoulos, Optimized pseudopotentials. *Phys. Rev. B* 1990, **41***,* 1227.

5. H. J. Monkhorst and J. Pack, Special points for Brillouin-zone integrations. *Phys. Rev. B,* 1976, **13***,* 5188.